Int. J. Electrochem. Sci., 17 **(2022)** Article Number: 221293, doi: 10.20964/2022.12.85

International Journal of
ELECTROCHEMICAL
SCIENCE
www.electrochemsci.org

High sensitive label-free electrochemical sensor using polydopamine-coated Zr-MOF composites for rapid detection of amoxicillin

Ying Wang and Liya Zhang[*]

Department of Pharmacy, The First Affiliated Hospital of China Medical University, Shenyang 110001 P.R. China
[*]E-mail: 634272796@qq.com

Received: 3 November 2022 / *Accepted:* 2 December 2022 / *Published:* 27 December 2022

In recent years, with the misuse and uncontrolled release of antibiotics, the detection of antibiotics has become an important area of research in analytical chemistry. This work utilizes the self-polymerization property of dopamine in alkaline solution to synthesize polydopamine-coated Zr-MOF composites (Zr-MOF-PDA) using zirconium-based metal-organic framework (Zr-MOF) of ligand 4-carboxyphenylporphyrin as the carrier material. The electrochemical sensor for highly sensitive detection of amoxicillin (AMO) was successfully constructed by drop coating this compliant material on the surface of glassy carbon electrode. The AMO was detected by differential pulse voltammetry under the optimized experimental conditions. The linearity range was 0.25~90 μM, and the detection limit was 71 nM. The sensor was successfully used to determine AMO in river water and tap water samples with good recovery. The proposed sensor provides a feasible solution for the sensitive detection of AMO.

Keywords: Metal organic framework; Polydopamine; Amoxicillin; Electrochemical sensor; Label-free

1. INTRODUCTION

Antibiotics are chemical substances that are widely used clinically in the treatment of diseases and can be extracted from microorganisms in nature as well as synthesized. Penicillin was first discovered by microbiologist Fleming in 1929 [1]. The development of antibiotics began in 1939 when pathologist Florey further realized the extraction and purification of penicillin [2]. At the same time, the development of theories such as biochemistry, microbiology, and molecular genetics has driven the development of antibiotics. Antibiotics are becoming an effective means of treating diseases caused by bacterial or microbial infections, but there is a growing problem of overuse of antibiotics [3–5]. The abuse of antibiotics can cause gastrointestinal disorders, affect organ function and the nervous system,

among other adverse effects. At the same time, antibiotics can gradually increase bacterial resistance to the entire ecosystem, leading to the worldwide problem of "superbacteria" [6–8].

Amoxicillin (AMO), with the molecular formula $C_{16}H_{19}N_3O_5S$, is a penicillin broad-spectrum antibiotic with extremely strong bactericidal effect. It is also highly absorbed by the gastrointestinal tract and is very effective in treating respiratory tract infections, reproductive system infections and typhoid fever [9–11]. Overdose can lead to serious consequences such as allergic reactions, metabolic reactions, and liver and kidney dysfunction [12]. In recent years, with the gradual progress of science and technology and the increasing concern for food safety, various antibiotic detection methods have been proposed one after another [13,14]. At present, the common techniques for the detection of antibiotics at home and abroad include high performance liquid chromatography (HPLC), high performance liquid chromatography-tandem mass spectrometry, immunoassay and microbiological assay [15–18].

HPLC is currently the most widely used detection method for veterinary drug residue analysis, with high selectivity, good stability and reproducibility, few false positives, rapid analysis, and quantitative detection [19–21]. Boguslaw Buszewski et al.[22] established a new HPLC-UV method for the rapid determination of AMO in human plasma by solid-phase microextraction (SPME). The results showed good linearity of AMO concentration in the range of 1-50ug/ml. The relative standard deviations (RSDs) results showed RSDs ≤5.9%. The plasma AMO was able to maintain stability for 8 hours at room temperature of 20^{o}C. The limits of detection and limits of quantification of this method were 1.21 μg/mL and 3.48 μg/mL, respectively. Liquid mass spectrometry (LCMS) reflects the complementary advantages of chromatography and mass spectrometry [23–25]. It combines the advantages of MS with its high sensitivity and ability to provide molecular mass and structure information, its high selectivity and the high separation ability of chromatography for complex samples. This has led to a wide range of applications in many fields such as pharmaceutical analysis, environmental analysis and food analysis. Sara Bogialli et al.[26] established a simple and rapid method for the detection of AMO and ampicillin in muscle, liver, kidney and milk of beef cattle. The method is based on matrix solid-phase dispersion technique with LC-MS technique. The aqueous phase extract was processed by acidification and filtration to inject 25 μL of tissue extract and 50 μL of milk extract into the LC. The absolute recoveries of both analytes ranged from 74 to 95% (RSD < 9%) at a spiked concentration of 50 ppb in blank tissue extract and at a spiked concentration of 4 ppb in blank milk extract. When penicillin V was used as an internal standard, the relative recoveries of the two target compounds ranged between 100 and 106% (RSD < 11%) at the spiked concentrations of 25 ppb and 2 ppb for tissue and milk extracts, respectively. The limits of quantification for these two analytes were less than 1 ppb in milk, and in beef cattle tissues they were quantified at 3.1 ppb and 0.8 ppb, respectively. Tim Reyns et al.[27] administered AMO (20 mg/kg) and AMO clavulanic acid (20 mg/kg and 5 mg/kg) orally and intravenously to pigs alone to study the residual elimination process of AMO and its major metabolites (AMA, DIKETO). Animals were slaughtered 12, 36, 48, 60, 72, and 84 h after administration and analyzed using LC-MS/MS techniques. The kidneys contained high concentrations of AMA, which was also eliminated at a slower rate than AMO. The measured concentrations of AMA were significantly higher in the liver and kidney under oral conditions than under intravenous conditions, and the concentrations of AMA in tissues were not significantly different under concomitant administration (AMO + clavulanic acid) than under single administration of AMO.

In addition, electrochemical sensors are used for AMO detection because of the advantages of small instrument size, simple operation, fast response and high sensitivity. Metal organic frameworks (MOFs) are a new class of porous functional materials formed by metal ions and organic ligands with excellent properties of tunable structure, large specific surface area and high porosity [28,29], and some MOFs also have good electrical conductivity and are therefore used as substrate materials to improve the electrical conductivity and sensitivity of electrochemical sensors [30,31]. In addition, carrier composites of polydopamine (PDA) can be prepared by in situ spontaneous oxidative polymerization of dopamine (DA) on carbon nanotubes [32], graphene oxide [33], titanium dioxide [34] and gold nanoparticles [35] materials in alkaline solution. In this paper, polydopamine-coated Zr-MOF composites (Zr-MOF-PDA) were synthesized using a Zr-MOF of the ligand 4-carboxyphenylporphyrin as the carrier material by taking advantage of the self-polymerization of dopamine in alkaline solutions. The electrochemical sensor for highly sensitive detection of AMO was successfully constructed by applying this compliant material and its drop coating on the surface of glassy carbon electrode. We characterized Zr-MOF-PDA using FTIR, thermogravimetric analysis, and SEM. The Zr-MOF-PDA /GCE electrochemical sensor has a wide linear range, low detection limits, good repeatability and interference immunity for AMO detection. Therefore, this study constructs a novel, low-cost electrochemical sensing platform for the quantitative determination of AMO.

2. EXPERIMENTAL

2.1. Reagents and instruments

PCN-223(H) (Zr-MOF) was purchased from Shanghai Kaixin Chemical Technology Co. Dopamine hydrochloride, amoxicillin, Tris-HCl, and sodium hydroxide were purchased from Aladdin Reagent Co. Chloramphenicol and sodium penicillin G were purchased from Tokyo Kasei Kogyo Co. Disodium hydrogen phosphate (Na_2HPO_4) and sodium dihydrogen phosphate (NaH_2PO_4) were prepared as phosphate buffer solution (PBS, 0. 1 M).

Hitachi S-4800 scanning electron microscope (Hitachi, Japan) is used for morphological feature observation. The NEXUS470 infrared spectrometer (Thermoelectric Nico Force, USA) was used for FTIR spectra acquisition, the TGA/STA-309 (Lindsay, Germany) was used for thermogravimetric analysis, and the CHI660D electrochemical workstation (Shanghai Chenhua Instruments) was used for electrochemical testing. A 3 mm diameter glassy carbon electrode (GCE) was used as the working electrode, a saturated glycury electrode as the reference electrode, and a platinum wire electrode as the counter electrode.

2.2. Preparation of Zr-MOF-PDA

Add 10 mg of Zr-MOF and 30 mL of water to a 100 mL round bottom flask and sonicate for 20 min to disperse it well. Add 30 mg of dopamine hydrochloride and 30 mL of Tris-HCl buffer (10 mmol/L, pH 8. 5), and stir the mixture at room temperature for 12 h. Wash with water and centrifuge

three times, and dry overnight at 30 ℃ to obtain the product. The synthesis procedure of PDA was the same as that of Zr-MOF, except that Zr-MOF was not added.

2.3. Sensor fabrication

GCE was polished and dried. 3 mg of Zr-MOF-PDA was dispersed in 1 mL of polyetherimide (PEI) solution (1%, mass fraction, prepared in water), and then 5 μL of 3 mg/mL Zr-MOF-PDA solution was Zr-MOF-PDA/GCE was prepared by drop coating on the GCE surface, and the Zr-MOF-PDA/GCE sensor was constructed by air-drying at room temperature. Other sensors were constructed using similar methods. Zr-MOF-PDA/GCE was immersed in PBS solution containing AMO and adsorbed for 6 min before differential pulse voltammetry (DPV) measurement.

3. RESULTS AND DISCUSSION

Figure 1 shows the the construction of electrochemical sensors and the self-polymerization process of DA. The Zr-MOF-PDA material was first synthesized under alkaline conditions, and then the Zr-MOF-PDA/GCE sensor was prepared by drop coating it on GCE. During the autopolymerization of DA, DA is first oxidized to the quinone structure. Then the quinone DA undergoes intramolecular cyclization via 1,4-michael addition reaction to obtain the more oxidizable 5,6-dihydroxyindoline. It undergoes oxidation and intramolecular rearrangement to form 5,6-dihydroxyindoline and its isomers, which further undergoes polymerization to obtain PDA.

Figure 1. Scheme of construction of electrochemical sensor and electrochemical sensing of AMO.

Figure 2 shows the FTIR spectra of Zr-MOF, PDA, Zr-MOF-PDA, BPA and Zr-MOF-PDA after adsorption of AMO. 3,442, 1,795 and 1,603 cm^{-1} in Zr-MOF are the O-H, C=O and C= C stretching vibrational peaks of the ligand 4-carboxyphenylporphyrin [36,37], respectively. 3,441, 1,627 and 1,402 cm^{-1} in PDA are the O-H, C= C and C-N stretching vibrational peaks of dopamine monomer, respectively. Zr-MOF-PDA possesses the characteristic peaks of Zr-MOF and PDA, indicating the successful synthesis of Zr-MOF-PDA composites. The adsorption of AMO by Zr-MOF-PDA resulted in enhanced O-H and C=C stretching vibrational peaks at 3415 and 1613 cm^{-1} [38,39].

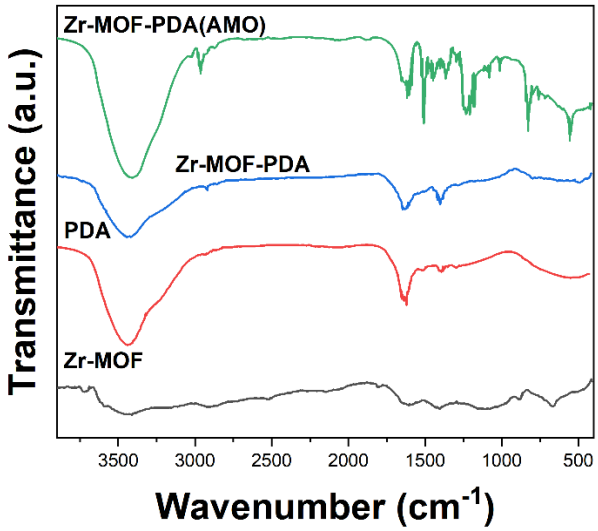

Figure 2. FTIR spectra of Zr-MOF, PDA, Zr-MOF-PDA and Zr-MOF-PDA adsorbed AMO.

Figure 3A shows the thermogravimetric analysis of Zr-MOF, PDA, Zr-MOF-PDA and Zr-MOF-PDA after adsorption of AMO. The weight losses of the four materials when heated to 1,000 °C were 36. 12%, 49.22%, 48. 81% and 51. 17%, respectively. The weight loss of Zr-MOF-PDA was in between Zr-MOF and PDA, indicating that Zr-MOF-PDA has been successfully synthesized [40]. The weight loss of Zr-MOF-PDA after adsorption of AMO was slightly larger than that of Zr-MOF-PDA, indicating that Zr-MOF-PDA had adsorption effect on AMO. SEM characterization of Zr-MOF-PDA was carried out (Figure 3B), and Zr-MOF-PDA was rod-shaped.

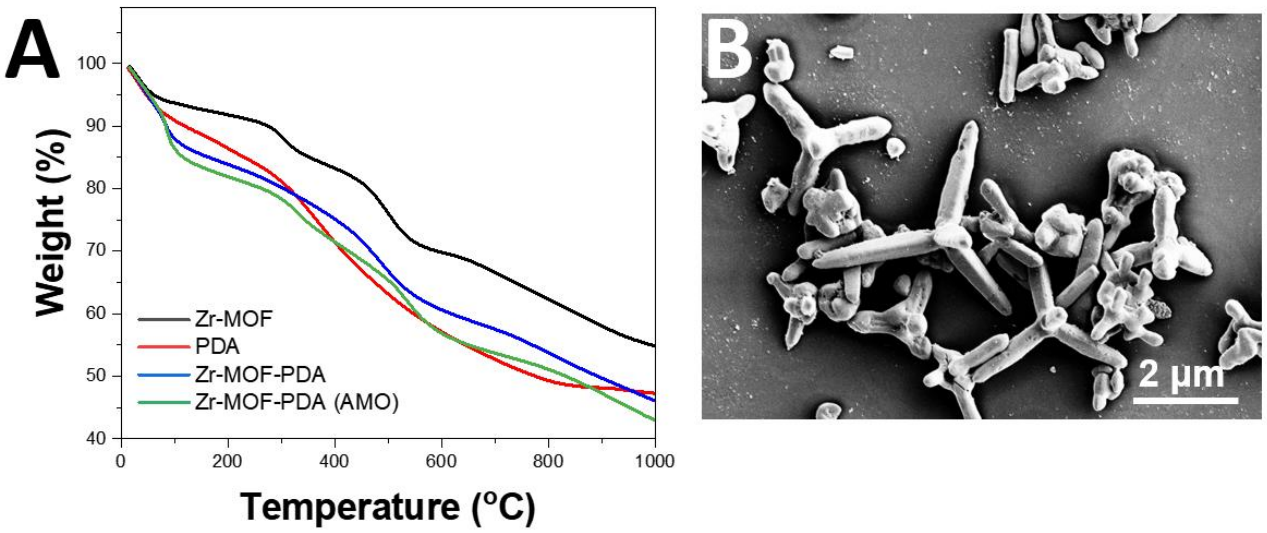

Figure 3. (A) TGA curves of Zr-MOF, PDA, Zr-MOF-PDA and Zr-MOF-PDA adsorbed AMO. (B) SEM image of Zr-MOF-PDA

The electrochemical behavior of bare GCE, Zr-MOF/GCE, and Zr-MOF-PDA/GCE was studied by cyclic voltammetry (CV) in 10 mL of solutions containing 5 mM $K_3[Fe(CN)_6]$ (0.1 M KCl). It can be seen from Figure 4 that the peak oxidation current values for Zr-MOF-PDA/GCE, Zr-MOF/GCE and bare GCE are 105.1, 93.21 and 72.69 μA, respectively. The oxidation peak current of Zr-MOF-PDA/GCE was larger than that of Zr-MOF/GCE, and the oxidation peak currents of the material-modified electrodes were all larger than that of bare GCE. This indicates that Zr-MOF-PDA has good electrical conductivity, which can accelerate the diffusion of $[Fe(CN)_6]^{3-/4-}$ on the electrode surface and promote its redox reaction [41].

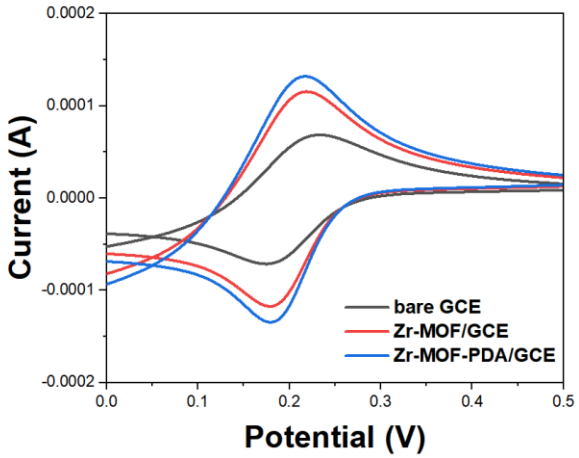

Figure 4. CV curves of bare GCE, Zr-MOF/GCE and Zr-MOF-PDA/GCE in 5 mM $K_3[Fe(CN)_6]$ + 0.1 M KCl (scan rate: 50 mV/s).

Timed Coulomb curves of the electrodes were studied in 10 mL of a solution containing 5 mM $K_3[Fe(CN)_6]$ (0.1 M KCl) (Figure 5A-B). The slopes of GCE, Zr-MOF/GCE, and Zr-MOF-PDA/GCE are 99.16, 142.41, and 105.12, respectively, according to the linear equation of $Q\text{-}t^{1/2}$. The corresponding effective surface areas of the electrodes were calculated by Anson's formula to be 0.471, 0.629, and 0.515 cm^2, respectively. The calculated results show that Zr-MOF/GCE has the largest effective surface area and Zr-MOF-PDA/GCE has a slightly smaller effective surface area. This may be due to the partial coverage of the holes on the surface after the Zr-MOF cladding on the PDA layer, but the effective surface area of both is larger than that of GCE [42]. This indicates that Zr-MOF-PDA has a large surface area, which can increase the adsorption of AMO, thus increasing the sensitivity of Zr-MOF-PDA/GCE for the detection of AMO [43].

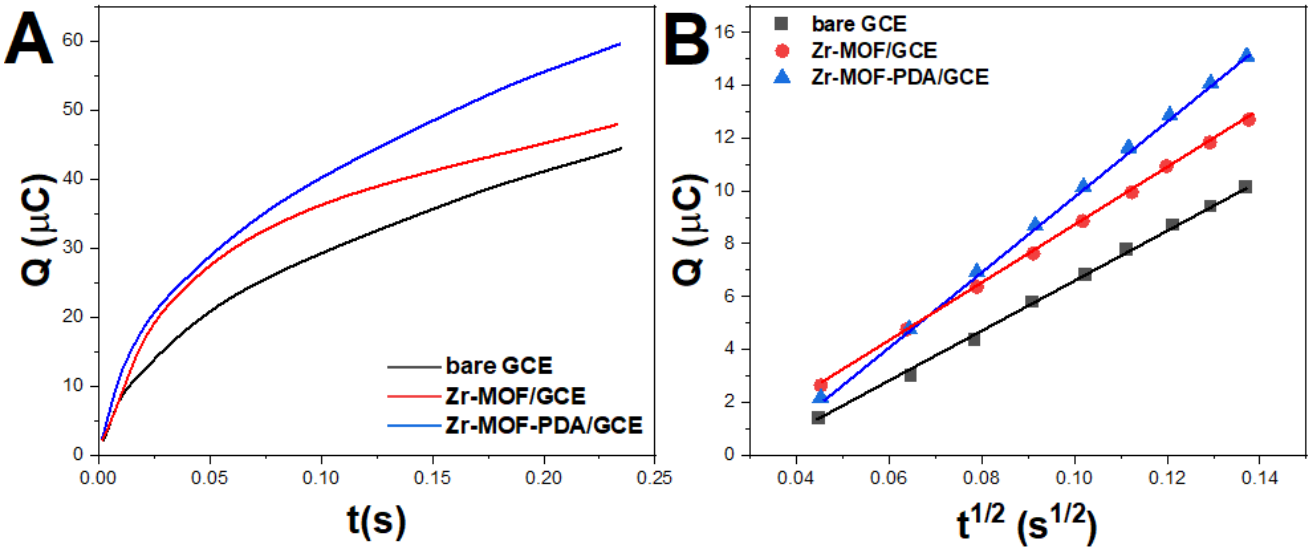

Figure 5. (A) Q-t and (B) Q-$t^{1/2}$ plots of bare GCE, Zr-MOF/GCE and Zr-MOF-PDA/GCE in 5 mM $K_3[Fe(CN)_6]$ (0. 1 M KCl).

In most of electrochemical studies of amoxicillin did not present any voltammetric signal of the unmodified electrodes [44,45], but only some of themwere able to display it, often with a not well-defined peak, which reflects their low sensitivity. The electrochemical behavior of GCE, Zr-MOF/GCE and Zr-MOF-PDA/GCE towards AMO was investigated. In addition, the CV response of Zr-MOF-PDA/GCE in AMO-free solution was experimentally investigated.

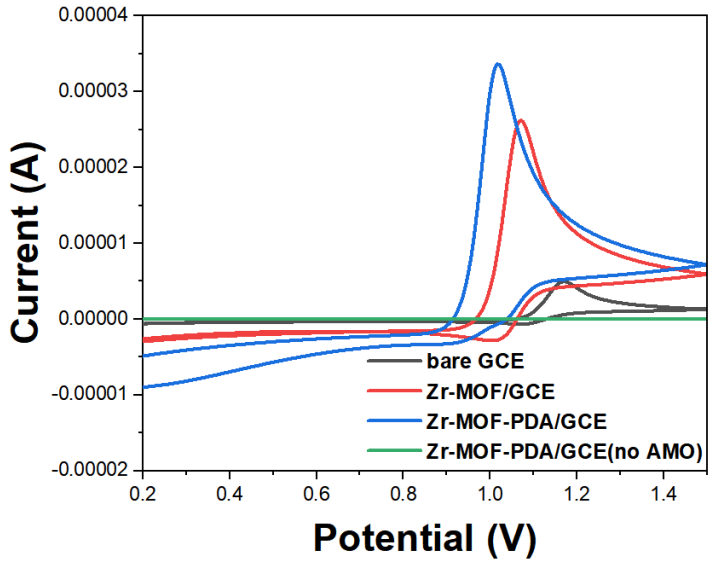

Figure 6. CV curve without AMO solution for Zr-MOF-PDA/GCE. CV curves of GCE, Zr-MOF/GCE and Z Zr-MOF-PDA/GCE with the presence of 80 μM AMO in 0.1 M PBS solution (pH 6.0) at scan rate of 100 mV/s.

As shown in Figure 6, the CV study showed that the analyte only showed an anodic peak signal, indicating that it underwent an irreversible oxidation process during the electrochemical detection. In addition, the electrochemical signal of AMO was significantly enhanced at the Zr-MOF-PDA/GCE-modified electrode by comparison with GCE, Zr-MOF/GCE and Zr-MOF-PDA/GCE. In the AMO-free solution, there was no peak current response, indicating that Zr-MOF-PDA/GCE can detect AMO more sensitively [46]. This can be attributed to its excellent electrochemical activity and excellent electrical conductivity to accelerate electron transfer [47]. The peak current value of AMO is related to the protonation process. Under neutral and alkaline conditions, the protonation of AMO is weak and the peak current decreases [25,48,49]. Therefore, pH 6.0 was selected in this experiment for the follow-up electrochemical sensing research of AMO.

The thickness of the sensing film significantly affects the electrode sensitivity and current response and can be controlled by varying the amount of Zr-MOF-PDA/GCE modified with GCE. The amount of Zr-MOF-PDA modification on GCE was optimized using the DPV technique in a supporting electrolyte of 0.1 M PBS (pH 6.0) containing 80 μM AMO as shown in Figure 7A-B. As the volume of Zr-MOF-PDA modification increased (from 2-10 μL), the oxidation peak current kept increasing. The peak current decreases when the dosage continues to increase because the film formed on the electrode surface is too thick, which hinders the transfer of electrons between the target analyte and the electrode and reduces the peak oxidation current [50]. Therefore, in this study, 10 μL of Zr-MOF-PDA was chosen to modify GCE.

The enrichment time plays a key role when measuring AMO on Zr-MOF-PDA/GCE (Figure 7C). For the target analytes, the peak current gradually increased as the enrichment time was extended from 0 to 2 min. When the enrichment time exceeded 2 min, the current first decreased and then stabilized. This means that the AMO enrichment reaches adsorption saturation on the electrode surface after 2 min and the peak current is maximum. Therefore, in the current work, 2 min are required for enrichment identification.

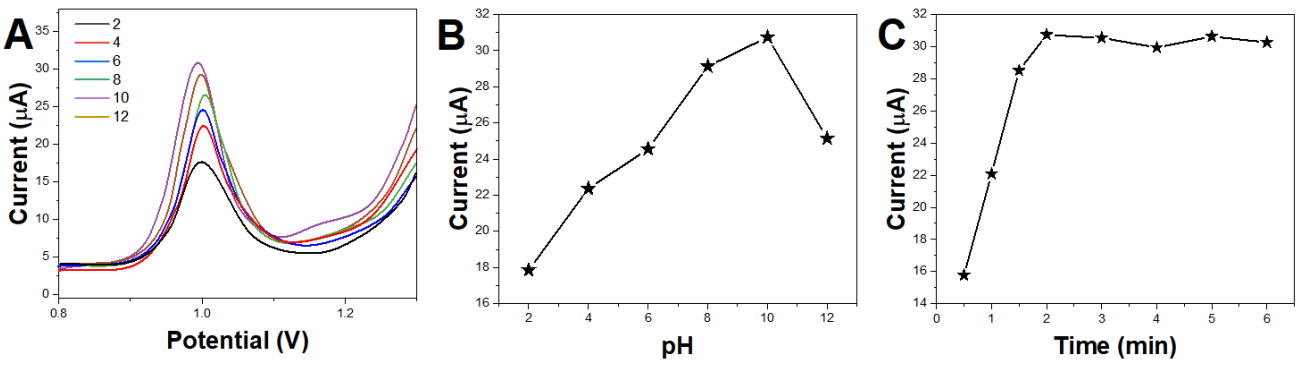

Figure 7. (A) The DPV response of Zr-MOF-PDA/GCE with different modifier. (B) Ip vs. modifier amount plots. (C) Influence of accumulation time towards 80 μM AMO detection in 0.1 M PBS at pH 6.0.

Under optimal experimental conditions, Zr-MOF/GCE was used for electrochemical detection of AMO in PBS solutions (pH 6.0) containing AMO (0.25-90 μM). As shown in Figure 8, the oxidation peak current increases with the increase of AMO concentration. The oxidation peak current showed a good linear relationship with the concentration of AMO in the concentration range of 0.25~10 μM and 10~90 μM. The presence of two linear ranges was due to the adsorption behavior at the electrochemical interface. At low concentrations, AMO molecules could be adsorbed as a monolayer on the Zr-MOF-PDA surface, producing a linear rage with higher sensitivity. At higher concentrations of AMO, adsorption was double layer or multilayer on the Zr-MOF-PDA surface and sensitivity was lower. The LOD of AMO was 73 nM (S/N=3). Comparison with other sensors reported in the literature for AMO detection is shown in Table 1, which shows that the sensing has a wide linear range and a low detection limit.

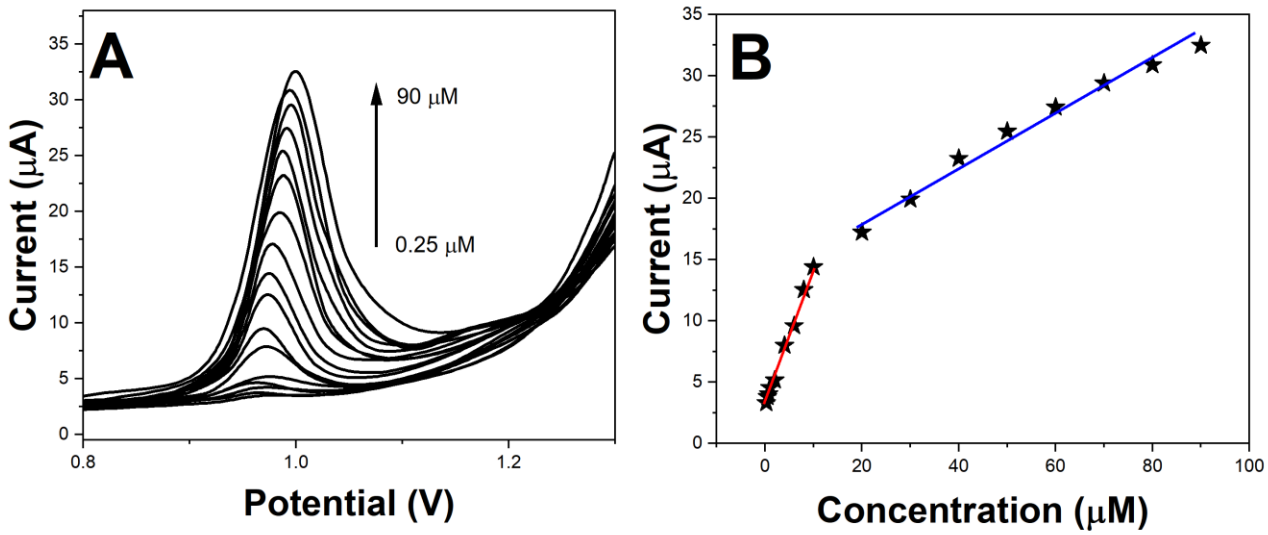

Figure 8. (A) DPVs of AMO at different concentrations from 0.25 to 90 μM in 0.1 M PBS (pH 6.0) on Zr-MOF-PDA/GCE and (B) corresponding linear calibration plots of oxidation peak currents for AMO with different concentrations.

Table 1. Comparison of Zr-MOF-PDA/GCE with previously reported AMO detection method.

Analytical method	Linear range	LOD	Reference
QDs-P6LC-PEDOT:PSS/GCE	0.90–69.0 μM	0.05 μM	[51]
CB/DPH/GCE	2.0–18.8 μM	0.12 μM	[52]
Ni/CR/CPE	8.0-100.0 μM	5.00 μM	[53]
MWCNT/GCE	0.6-8.0 μM	0.20 μM	[54]
AuNPs/en-(MWCNTs)/SPE	0.2-30 μM	0.015 μM	[55]
Zr-MOF-PDA/GCE	0.25-10 μM; 10-90 μM	71 nM	This work

Table 2. Determination of AMO in river water and tap water using proposed Zr-MOF-PDA/GCE.

Sample	Added (μM)	Found (μM)	Recovery (%)	RSD (%)
River water	-	0.00	-	-
	10.00	10.13	101.30	4.23
	30.00	28.99	96.63	3.66
Tap water	0.50	0.51	102.80	3.51
	1.00	0.96	95.50	2.47
	5.00	5.43	108.60	5.51

To evaluate the applicability of Zr-MOF-PDA/GCE, river water samples and tap water samples were selected for analysis. The river water samples and tap water samples were first pretreated with 0.45 μm filter membranes and diluted a certain number of times with PBS solution. Afterwards, the electrochemical response of DPV was recorded in river water and tap water samples after adding a quantitative amount of AMO. According to Table 2, it can be clearly seen that the average recoveries of the analytical results of the prepared sensors ranged from 95.5% to 108.6% with an RSD lower than 5.51%, indicating that Zr-MOF-PDA/GCE can be used for the detection of real samples.

4. CONCLUSION

In this study, the first Zr-MOF-PDA/GCE sensor was constructed for the detection of AMO. Zr-MOF-PDA was synthesized under mild and environmentally friendly conditions. Zr-MOF-PDA has a large surface area, fast electron transfer capability and excellent electrochemical properties. The proposed sensor is simple to prepare and has excellent electrochemical oxidation performance for AMO. The assay has a wide linear range and low detection limit. In addition, it has good application prospects and satisfactory recoveries. Therefore, the constructed electrochemical sensing platform has potential applications for the detection of AMO in pharmaceutical analysis.

References

1. F. Diggins, *Biol. Lond. Engl.*, 47 (2000) 115–119.
2. Y. Yang, G. Ren, W. Yang, X. Qin, D. Gu, Z. Liang, D.-Y. Guo, P. Qinhe, *Polyhedron*, 194 (2021) 114923.
3. G.-D. Wang, Y.-Z. Li, W.-J. Shi, B. Zhang, L. Hou, Y.-Y. Wang, *Sens. Actuators B Chem.*, 331 (2021) 129377.
4. Y. Zhang, B. Duan, Q. Bao, T. Yang, T. Wei, J. Wang, C. Mao, C. Zhang, M. Yang, *J. Mater. Chem. B*, 8 (2020) 8607–8613.
5. M. Wang, M. Hu, J. Liu, C. Guo, D. Peng, Q. Jia, L. He, Z. Zhang, M. Du, *Biosens. Bioelectron.*, 132 (2019) 8–16.
6. A.-G. Goubet, R. Daillère, B. Routy, L. Derosa, P. M. Roberti, L. Zitvogel, *C. R. Biol.*, 341 (2018) 284–289.
7. C.M. Lewis, A. Obregón-Tito, R.Y. Tito, M.W. Foster, P.G. Spicer, *Trends Microbiol.*, 20 (2012) 1–4.
8. A. Berstad, J. Raa, T. Midtvedt, J. Valeur, *Microb. Ecol. Health Dis.*, 27 (2016) 31557.

9. A. Wong, A.M. Santos, F.H. Cincotto, F.C. Moraes, O. Fatibello-Filho, M.D.P.T. Sotomayor, *Talanta*, 206 (2020) 120252.
10. A.A. Aryee, R. Han, L. Qu, *J. Clean. Prod.*, 368 (2022) 133140.
11. A. Hrioua, A. Loudiki, A. Farahi, M. Bakasse, S. Lahrich, S. Saqrane, M.A.E. Mhammedi, *Bioelectrochemistry*, 137 (2021) 107687.
12. W. Luo, C.Y. Ang, *J. AOAC Int.*, 83 (2000) 20–25.
13. O. Jamieson, T.C. Soares, B.A. de Faria, A. Hudson, F. Mecozzi, S.J. Rowley-Neale, C.E. Banks, J. Gruber, K. Novakovic, M. Peeters, *Chemosensors*, 8 (2019) 5.
14. J. Song, M. Huang, N. Jiang, S. Zheng, T. Mu, L. Meng, Y. Liu, J. Liu, G. Chen, *J. Hazard. Mater.*, 391 (2020) 122024.
15. D.K. Nguyen, C.-H. Jang, *Micromachines*, 12 (2021) 370.
16. N. Bereli, D. Çimen, S. Hüseynli, A. Denizli, *J. Food Sci.*, 85 (2020) 4152–4160.
17. L. Wang, G. Zhou, X. Guan, L. Zhao, *Spectrochim. Acta. A. Mol. Biomol. Spectrosc.*, 235 (2020) 118262.
18. X. Zhang, Y. Ren, Z. Ji, J. Fan, *J. Mol. Liq.*, 311 (2020) 113278.
19. M. Majdinasab, R.K. Mishra, X. Tang, J.L. Marty, *TrAC Trends Anal. Chem.*, 127 (2020) 115883.
20. M. Yu, Y. Xie, X. Wang, Y. Li, G. Li, *ACS Appl. Mater. Interfaces*, 11 (2019) 21201–21210.
21. M. Marimuthu, S.S. Arumugam, D. Sabarinathan, H. Li, Q. Chen, *Trends Food Sci. Technol.*, 116 (2021) 1002–1028.
22. B. Buszewski, M. Szultka, P. Olszowy, S. Bocian, T. Ligor, *Analyst*, 136 (2011) 2635–2642.
23. A. Joshi, K.-H. Kim, *Biosens. Bioelectron.*, 153 (2020) 112046.
24. F. Yue, F. Li, Q. Kong, Y. Guo, X. Sun, *Sci. Total Environ.*, 762 (2021) 143129.
25. J. Lu, M. Cheng, C. Zhao, B. Li, H. Peng, Y. Zhang, Q. Shao, M. Hassan, *Ind. Crops Prod.*, 176 (2022) 114267.
26. S. Bogialli, V. Capitolino, R. Curini, A. Di Corcia, M. Nazzari, M. Sergi, *J. Agric. Food Chem.*, 52 (2004) 3286–3291.
27. T. Reyns, S. De Boever, S. De Baere, P. De Backer, S. Croubels, *J. Agric. Food Chem.*, 56 (2008) 448–454.
28. Y. Zhong, B. Li, S. Li, S. Xu, Z. Pan, Q. Huang, L. Xing, C. Wang, W. Li, *Nano-Micro Lett.*, 10 (2018) 56.
29. A.E. Baumann, D.A. Burns, B. Liu, V.S. Thoi, *Commun. Chem.*, 2 (2019) 86.
30. C.-S. Liu, J. Li, H. Pang, *Coord. Chem. Rev.*, 410 (2020) 213222.
31. Y. Xue, S. Zheng, H. Xue, H. Pang, *J. Mater. Chem. A*, 7 (2019) 7301–7327.
32. W. Wu, L. Yang, F. Zhao, B. Zeng, *Sens. Actuators B Chem.*, 239 (2017) 481–487.
33. F. Tan, M. Liu, S. Ren, *Sci. Rep.*, 7 (2017) 5735.
34. H. Kan, M. Li, H. Li, C. Li, J. Zhou, C. Fu, J. Luo, Y. Fu, *RSC Adv.*, 9 (2019) 38531–38537.
35. J. Li, L. Liu, Y. Ai, Y. Liu, H. Sun, Q. Liang, *ACS Appl. Mater. Interfaces*, 12 (2020) 5500–5510.
36. L. Zhou, S. Wang, Y. Chen, C. Serre, *Microporous Mesoporous Mater.*, 290 (2019) 109674.
37. C. Wang, C. Xiong, Y. He, C. Yang, X. Li, J. Zheng, S. Wang, *Chem. Eng. J.*, 415 (2021) 128923.
38. A. Badoei-dalfard, A. Shahba, F. Zaare, G. Sargazi, B. Seyedalipour, Z. Karami, *Int. J. Biol. Macromol.*, 192 (2021) 1292–1303.
39. H. Gul Zaman, L. Baloo, S. Rahman Kutty, M. Altaf, *Arab. J. Chem.* (2022) 104122.
40. M.N. Nimbalkar, B.R. Bhat, *J. Environ. Chem. Eng.*, 9 (2021) 106216.
41. N. Gao, R. Tan, Z. Cai, H. Zhao, G. Chang, Y. He, *J. Mater. Sci.*, 56 (2021) 19060–19074.
42. H.-K. Li, H.-L. Ye, X.-X. Zhao, X.-L. Sun, Q.-Q. Zhu, Z.-Y. Han, R. Yuan, H. He, *Chin. Chem. Lett.*, 32 (2021) 2851–2855.
43. C.-H. Chuang, C.-W. Kung, *Electroanalysis*, 32 (2020) 1885–1895.
44. F. Sopaj, M.A. Rodrigo, N. Oturan, F.I. Podvorica, J. Pinson, M.A. Oturan, *Chem. Eng. J.*, 262 (2015) 286–294.
45. R. Ojani, J.-B. Raoof, S. Zamani, *Bioelectrochemistry*, 85 (2012) 44–49.

46. X. Weng, J. Huang, H. Ye, H. Xu, D. Cai, D. Wang, *Anal. Methods*, 14 (2022) 3000–3010.
47. X. Ma, C. Pang, S. Li, Y. Xiong, J. Li, J. Luo, Y. Yang, *Biosens. Bioelectron.*, 146 (2019) 111734.
48. Z. Wu, J. Liu, M. Liang, H. Zheng, C. Zhu, Y. Wang, *Front. Chem.*, 9 (2021) 208.
49. C. Li, F. Sun, *Front. Chem.*, 9 (2021) 409.
50. Q. Wang, C. Gu, Y. Fu, L. Liu, Y. Xie, *Molecules*, 25 (2020) 4557.
51. A. Wong, A.M. Santos, F.H. Cincotto, F.C. Moraes, O. Fatibello-Filho, M.D.P.T. Sotomayor, *Talanta*, 206 (2020) 120252.
52. P.B. Deroco, R.C. Rocha-Filho, O. Fatibello-Filho, *Talanta*, 179 (2018) 115–123.
53. R. Ojani, J.-B. Raoof, S. Zamani, *Bioelectrochemistry*, 85 (2012) 44–49.
54. B. Rezaei, S. Damiri, *Electroanalysis*, 21 (2009) 1577–1586.
55. A. Muhammad, N.A. Yusof, R. Hajian, J. Abdullah, *Sensors*, 16 (2016) 56.